Est. 1841 | YORK ST JOHN UNIVERSITY

Wang, Bangguo, Wang, Lijing, Cen, Wenxi, Lyu, Tao, Jarvis, Peter, Zhang, Yang, Zhang, Yuanxun, Han, Yinghui, Wang, Lei, Pan, Gang, Zhang, Kaili and Fan, Wei (2024) Exploring a chemical input free advanced oxidation process based on nanobubble technology to treat organic micropollutants. Environmental Pollution, 340 (1). p. 122877.

Downloaded from: https://ray.yorksj.ac.uk/id/eprint/8975/

The version presented here may differ from the published version or version of record. If you intend to cite from the work you are advised to consult the publisher's version: https://www.sciencedirect.com/science/article/abs/pii/S0269749123018791

Research at York St John (RaY) is an institutional repository. It supports the principles of open access by making the research outputs of the University available in digital form. Copyright of the items stored in RaY reside with the authors and/or other copyright owners. Users may access full text items free of charge, and may download a copy for private study or non-commercial research. For further reuse terms, see licence terms governing individual outputs. Institutional Repositories Policy Statement

RaY

Research at the University of York St John

For more information please contact RaY at ray@yorksj.ac.uk

# Exploring a chemical input free advanced oxidation process based on nanobubble technology to treat organic micropollutants

Bangguo Wang[1], Lijing Wang[1]*, Wenxi Cen[1], Tao Lyu[2], Peter Jarvis[2], Yang Zhang[1], Yuanxun Zhang[1,3], Yinghui Han[1], Lei Wang[4], Gang Pan[5,6], Kaili Zhang[7], Wei Fan[8]

[1]*College of Resources and Environment, University of Chinese Academy of Sciences, Beijing, 101408, China*
[2]*School of Water, Energy and Environment, Cranfield University, College Road, Cranfield, Bedfordshire MK43 0AL, United Kingdom*
[3]*Yanshan Earth Critical Zone and Surface Fluxes Research Station, University of Chinese Academy of Sciences, Beijing, 101408, China*
[4]*Research Centre for Eco-environmental Sciences, Chinese Academy of Sciences, 18 Shuangqing Road, Beijing, 100085, China*
[5]*School of Humanities, York St John University, Lord Mayor's Walk, York, North Yorkshire YO31 7EX, United Kingdom*
[6]*School of Chemical and Environmental Sciences, Guangdong Ocean University, Zhanjiang, 524088, China*
[7]*Binzhou Institute of Technology, 8 Huanghe Road, Binzhou 256606, China*
[8]*School of Environment, Northeast Normal University, 2555 Jingyue Street, Changchun 130117, China*

*Corresponding authors: wanglijing@ucas.ac.cn (*L.W.*); t.lyu@cranfield.ac.uk (*T.L.*)

## Abstract

Advanced oxidation processes (AOPs) are increasingly applied in water and wastewater treatment, but their energy consumption and chemical use may hinder their further implementations in a changing world. This study investigated the feasibility and mechanisms of the chemical-free nanobubble-based AOP for treating organic micropollutants in both synthetic and real water matrices. The removal efficiency of the model micropollutant Rhodamine B (RhB) by oxygen nanobubble AOP (98%) was significantly higher than air (73%) and nitrogen nanobubbles (69%). The treatment performance was not significantly affected by initial RhB concentrations (0.1-10 mg/L), pH (3-10), and existing ions ($Ca^{2+}$, $Mg^{2+}$, $HCO_3^-$, and $Cl^-$). Both qualitative and quantitative analysis of reactive oxygen species (ROSs) using the fluorescent probe, electron spin resonance, and quenching experiments demonstrated the contributions of ROSs in RhB degradation followed the order: hydroxyl radical (•OH)> superoxide radical ($•O_2^-$)> singlet oxygen ($^1O_2$). The cascade degradations of RhB were identified, involving N-deethylation, hydroxylation, chromophore cleavage, opening-ring and complete mineralisation. Moreover, the treatment of real water samples, including natural lake

water and sewage work's secondary effluent, showed considerable RhB removals (75.3%-90.8%), supporting its practical feasibility. Overall, the results benefit future research and application of chemical free nanobubble-based AOP for water and wastewater treatment.

**Keywords:** Micro/nanobubble technology, green technology, reactive oxygen species, organic micropollutant, water and wastewater treatment

## 1. Introduction

Numerous persistent micropollutants resulting from farming practices, industrial and household effluents have been identified in rivers and lakes globally (Devi et al., 2013; Xia et al., 2023). These micropollutants can pose significant risks to human health and ecological safety, even at trace concentrations (Murtaza et al., 2023; Yang et al., 2022). Advanced oxidation processes (AOPs), such as ozonation (van Gijn et al., 2022), photocatalysis (Zeng et al., 2022), and Fenton reaction (Zhang et al., 2022). have been successful in removing organic micropollutants during water and wastewater treatment. However, those processes usually require energy consumption and the use of hazardous chemicals such as ozone, peroxide, and/or UV light. Moreover, unwanted by-products (e.g. Fenton sludge) could be generated and lead to increased operational costs (Muthusami et al., 2021). To mitigate the environmental impact of the conventional AOPs, there is an urgent need to develop sustainable, cost-effective, and chemical-free alternatives.

Nanobubbles are gas cavities in the aqueous phase with diameters smaller than 1000 nm that possess unique physicochemical properties compared to conventional bubbles. These properties include a long lifespan, large specific surface area, low buoyancy, aggregated gas density, and negative surface charge (Lyu et al., 2019; Wang et al., 2020). As a result, nanobubbles have been employed in diverse fields, such as medicine delivery (Hernandez et al., 2019), crop yield enhancement (Wu et al., 2019), food processing (Thi Phan et al., 2020), and environmental remediation (Hu and Xia, 2018; Wang et al., 2018). In water and wastewater treatment, nanobubble technology has demonstrated superior performance in improving biological and physiochemical treatment processes, leading to better removal of nutrients (Zhang et al., 2021), biofouling (Fan et al., 2021b), taste and odour compounds (Soyluoglu et al., 2022), and organic micropollutants (Fan et al., 2021a). The current concepts of using nanobubble technology in

AOPs has been mainly through the incorporation of nanobubbles with other AOPs to intensify the overall treatment performance. For instance, the removal efficiencies of oxytetracycline (Wang et al., 2020) and bacterial spores (Fan et al., 2021b) were significantly increased by adopting nanobubbles in photocatalytic processes. Similarly, adding nanobubbles in $H_2O_2$ based reaction improved the production of ROSs and enhanced the degradation of a fabric dye (Bui and Han, 2020). Previous studies to date concluded that nanobubbles can reduce chemical usage and energy consumption in AOPs on the premise of achieving an equivalent treatment performance. These applications align with a view that the generation of ROSs from nanobubbles can occur under external stimulations, such as the metal catalysis and UV light stimulations from incorporated AOPs. Nevertheless, recent studies have shown that ROSs can also be generated in solutions under ambient unstimulated conditions during the treatment process (Ji et al., 2020). Therefore, whether and to what extent the nanobubble technology can be used alone as a chemical-free AOP for water and wastewater treatment need to be investigated.

In conventional AOPs, pH is an essential factor that influences the treatment performance. The efficacy of homogeneous Fenton reactions is usually higher under acidic conditions (Liu et al., 2021), while the effects of pH on heterogeneous AOPs are determined by the properties of catalysts and pollutants (Akpan and Hameed, 2009). Besides pH, other water quality parameters, such as ionic strength, hardness, and alkalinity, could also reduce the favourable oxidation ability of AOPs by potential quenching effects on ROSs (Liao et al., 2001; Yu et al., 2021). Thus, it is crucial to assess the potential influencing factors on the proposed nanobubble-based AOP approach. While some developed AOPs can generate ROSs for the destruction of parent micropollutant compounds, the ROSs may not be sufficient to entirely mineralise the molecules (Tran et al., 2021; Zeng et al., 2022). Moreover, many AOPs development studies were tested using synthetic water samples, while lacking further validation in real-world water matrices. Therefore, comprehending the degradation pathways of micropollutants and validating the process in actual water samples are crucial to evaluate the effectiveness of the proposed nanobubble-based AOP approach.

To explore the feasibility of nanobubble-based chemical input free AOP for water and wastewater treatment, the degradation of the target model compound Rhodamine B (RhB) was investigated in both synthetic and real water matrices. The impacts on the treatment performance by potential influencing factors, including initial RhB concentration (0.1-10 mg/L), pH (3-10), and existing ions ($Ca^{2+}$, $Mg^{2+}$, $HCO_3^-$, and $Cl^-$), were assessed. The generation and contribution of different ROSs on RhB degradation were qualitatively and quantitatively analysed using the fluorescent probe, electron spin resonance, and quenching experiments. Moreover, the primary contributing ROS, i.e. hydroxyl radical (•OH), was monitored and visualized by the three-dimensional excitation and emission matrix (EEM) fluorescence spectra. The intermediate by-products were identified to reveal the degradation pathways of RhB. Finally, the perspectives of extrapolating the current findings to other applications and future research needs were discussed.

# 2. Materials and Methods

## 2.1 Nanobubble preparation and characterisation

Nanobubbles were generated using a commercial nanobubble generator (Shanghai Zhongchen Digital Technology Equipment Co., Ltd., Shanghai, China) with a power of 0.25 kW. The concentration, mean size, and size distribution of the nanobubbles were detected using a nanoparticle tracking analysis system (Nanosight NTA NS500, Malvern Instrument Co., Ltd. UK). The zeta potential of the nanobubbles was determined by Zetasizer Nano ZS (90Plus PALS, Malvern Instrument Co., Ltd. UK). Dissolved oxygen (DO) was measured using a DO probe (JPBJ-608, INESA Scientific Instrument Co., Ltd. China).

## 2.2 Initial degradation experiments

Certain amount of RhB, as the target organic micropollutant, was spiked into a reaction tank filled with 8 L of deionised (DI) water, resulting in initial concentrations of 0.1, 1 and 10 mg/L. The degradation processes occurred in a homogeneous system, where bulk nanobubbles were continuously generated and introduced into the RhB solutions throughout the reaction duration. Water samples were collected at intervals during the experiment, and the concentration of RhB was determined using a UV spectrophotometer (Varian Cary 60, Agilent Technologies Co., Ltd.

USA). The total organic carbon of the solutions was measured by a TOC analyzer (Multi N/C 3100, Analytik Jena AG Co., Ltd. German). The details about used chemicals and degradation experiments are provided in the supplementary material (**Text S1 and S2**).

### 2.3 Influencing factors on the effectiveness of the nanobubble-based AOP

Separated experiments were conducted to evaluate the impact of pH and existing ions on the degradation of RhB using nanobubble-based AOP treatment. HCl and NaOH were used to adjust the initial pH values from 3 to 10 before treatment. Moreover, NaCl, $NaHCO_3$, $CaCl_2$, and $MgCl_2$ were used to obtain different levels of ironic strength, alkalinity, and hardness in the initial solution. The same sampling and analysis procedures used in the initial degradation experiment were followed.

### 2.4 Micropollutant removal mechanisms and degradation pathways

The contributions of different ROSs to the degradation of RhB were examined through a series of quenching experiments. The generation of •OH was further qualitatively detected by electron spin resonance (ESR) (EMXplus, X-band, Brucker Analytical Instruments Co., Ltd. German). In addition, fluorescent probe method was employed to monitor the generation of •OH along the time via the three-dimensional emission matrix fluorescence (EEM) spectra and quantitatively measure the production of •OH in the experimental system via the calibration curve (Soyluoglu et al., 2021; Fang et al., 1996). Besides monitoring the changes of the parent compound of RhB, the degradation intermediates of RhB were identified by Ultra High Performance Liquid Chromatography (Ultimate 3000 UHPLC, Dinonex Co., Ltd, USA) with Q Exactive mass spectra (MS, Thermo Fisher Scientific Co., Ltd, USA). The degradation pathway of RhB was then proposed based on those intermediates. Details regarding the setup of the UHPLC and fluorescent probe method are provided in the supplementary material (**Text S3 and S4**).

### 2.5 Further validations using real water matrices.

To validate the proposed nanobubble-based AOP, experiments were further conducted using four different water matrices, including i) deionized water; ii) tap water; iii) natural lake water collected from Yanqi Lake in Beijing, which serves as an important source of drinking water

and scenic spot, and iv) secondary effluent from Bishui Wastewater Treatment Plant in Beijing. RhB was spiked at a concentration of 1 mg/L into those water samples, and the experimental setup and sampling processes were similar to the details in the initial degradation experiments.

# 3. Results and Discussion

## 3.1 Nanobubble size, distribution and longevity

Nanobubble was generated by hydrodynamic cavitation method, which was deemed the most efficient way to produce a large number of bulk nanobubbles suitable for water and wastewater treatment (Lyu et al., 2019). Before operating the bubble generator, the ultrapure water contained bubbles that had an average size > 1 μm, while fewer than $10^5$ particles/mL in the nanoscale range (**Fig. 1a**). After 10 minutes operation of the generator, nanobubbles with an average size of 192±15 nm and a concentration of $4.2\times10^7$ particles/mL were produced (**Fig. 1b**). After turning off the generator, the stabilisation of the nanobubbles was monitored for 72 hrs. The average size of nanobubbles slightly increased with time and reached 232±14 nm after 72 h (**Fig. 1c-f**), likely from the fusion of nanobubbles (Wang et al., 2020). This was consistent with a small drop in bubble concentration between the beginning and end of the time period ($4.2\times10^7$ to $3.8\times10^7$ particles/mL, **Fig. 1f**). The results indicated that nanobubbles possessed significant longevity in water, which was in accordance with previous studies that have reported that nanobubbles can exist in water for several weeks and even months (Soyluoglu et al., 2021; Wang et al., 2020). The gas inside nanobubbles may exist as an aggregation and the diffusion of the gas into the nanobubbles is likely to be slow and take place over a long period of time. Notably, the speed of gas dissolution would accelerate during the treatment process from the presence of pollutants and/or under anaerobic conditions due to the external stimulus induced nanobubble collapse (Ji et al., 2020). The unique characteristics of longevity and strengthened gas utilisation efficiency provide nanobubbles with the potential to significantly enhance water and wastewater treatment.

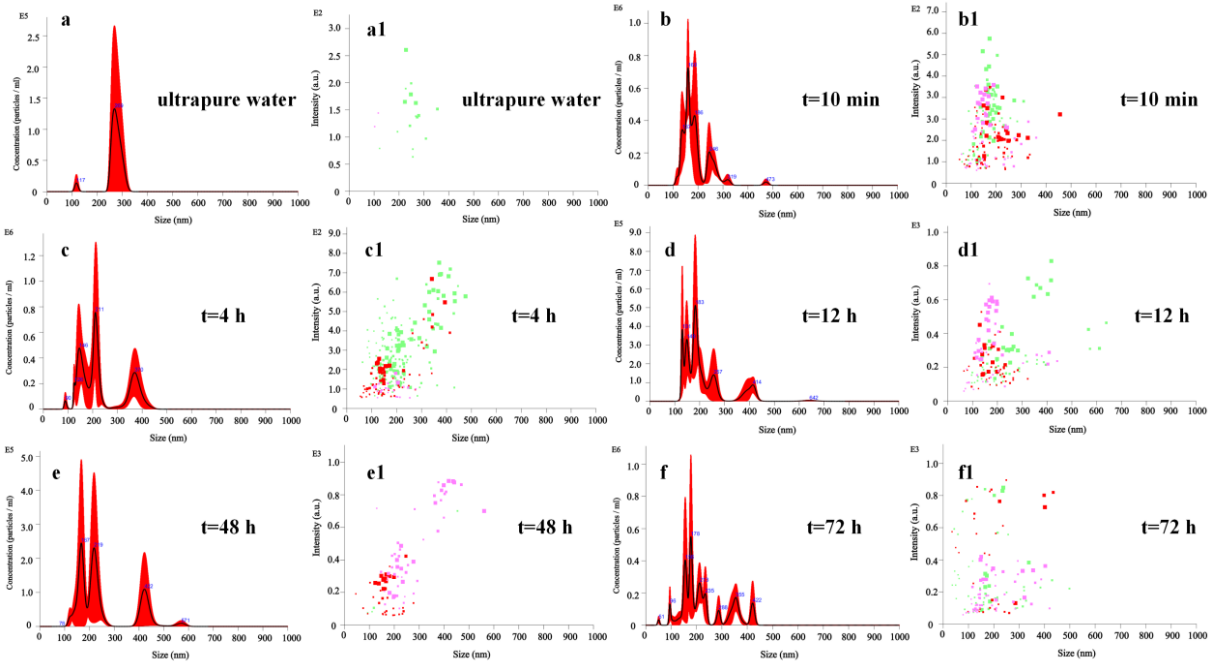


**Fig. 1.** The size and distribution of nanobubbles in ultrapure water (a) and the prepared nanobubble water at 10 min (b), 4h (c), 12h (d), 48h (e), and 72h (f). The operation time of the generation was 10 mins. Different colours in the intensity/size graphs (a1-f1) represent the results from three separate measurements.

### 3.2 Screening test of different nanobubble treatments for the micropollutant removal

Previous studies have reported that oxygen aeration through common diffusers can increase the photocatalytic removal of RhB, which was attributed to the enhancement of •OH generation (Lee et al., 2013). In this study, without the assistance of other AOP technologies, the conventional oxygen aeration treatment could only obtain approximately 19% removal of RhB after 120 mins for an initial concentration of 1 mg/L (**Fig. 2a**). However, under the same conditions, nearly complete removal (98%) of RhB was achieved in the oxygen nanobubble treatment group. It may be due to the rapidly increased charge density of the surface electric double-layer on nanobubbles during the continuous shrinkage process (Agarwal et al., 2011). Thus, massive energy could instantaneously be released when nanobubbles collapse and form an extremely high temperature and pressure condition in the ambient area, which was sufficient to break the O-H bond of water molecules and induce ROSs generation (Agarwal et al., 2011). The generated ROSs contributed to the oxidisation of RhB compounds in this study, similar to the degradation process in other AOPs.

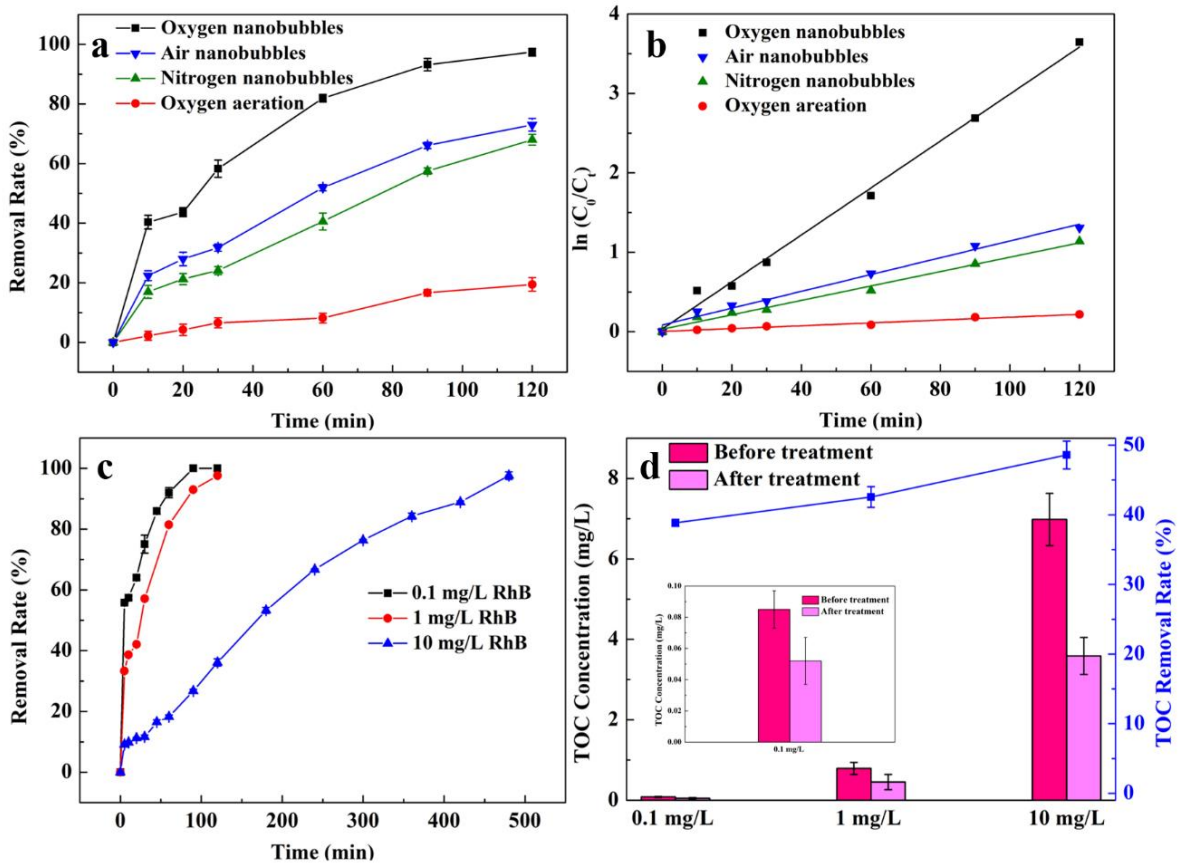


**Fig. 2.** The remove rates of RhB along with the experiment treated by oxygen, air, nitrogen nanobubbles and conventional oxygen aeration process (a), as well as the fitted first-order kinetics models (b), the removal rate of RhB under the oxygen nanobubbles treatment with different RhB initial concentrations (c), the initial and final concentrations of TOC in all treatment groups (d).

Besides oxygen nanobubbles, other gases-filled nanobubbles, such as air and nitrogen, can also generate ROSs and have previously been shown to follow the order reactivity of oxygen > air > nitrogen (Ahmed et al., 2018). The current findings support that view for the degradation of RhB by nanobubbles, which decreased the degradation rate in the order of oxygen (98%), air (73%), and nitrogen (68%) nanobubbles (**Fig. 2a**). The pseudo-first-order kinetics model described the degradation reactions in all groups ($R^2$>0.90) and the reaction rate constants (k) for each group also exhibited same trend as degradation rate (**Fig. 2b**, **Table S1**). This result was consistent with previous studies that investigated the effects of different gas-filled nanobubbles on the degradation of taste and odour compounds (Soyluoglu et al., 2022) and phenol (Li et al., 2009) from water.

### 3.3 Removal mechanisms and degradation pathways of the micropollutant

### *3.3.1 ROSs-based degradation mechanism*

Understanding the removal mechanisms of RhB by oxygen nanobubble AOP is crucial to direct future technology development and implementation. Quenching experiments were conducted to ascertain the contribution of individual reactive species, including •OH, $•O_2^-$, and $^1O_2$, during the degradation process. The removal rate of RhB decreased from 98% to 46%, 56%, and 68% when the •OH, $•O_2^-$, and $^1O_2$ were quenched, respectively (**Fig. 3a**, **Table S2**). The results supported the view that •OH, $•O_2^-$, and $^1O_2$ coexisted in the nanobubble solution (Liu et al., 2016), and all ROSs could contribute to the degradation of RhB. Moreover, the contribution of different ROSs to RhB degradation by oxygen nanobubbles followed the order of •OH > $•O_2^-$ > $^1O_2$. Previous studies have also indicated that •OH was the most important oxidant in the oxygen nanobubble system for the degradation of oxytetracycline (Wang et al., 2020) and phenol (Li et al., 2009). To further verify the primary role of •OH in the degradation process, the ESR technique was employed to qualitatively detect the generated •OH. The results show that when 5,5-dimethyl-1-pyrroline-N-oxide (DMPO) was chosen as the spin-trap reagent, there was no significant signal corresponding to •OH in the DI water (**Fig. 3b**). However, an ESR spectrum of DMPO-•OH, containing four peaks with intensity ratios of 1:2:2:1 was detected in the oxygen nanobubble water, indicating the generation of •OH radical.

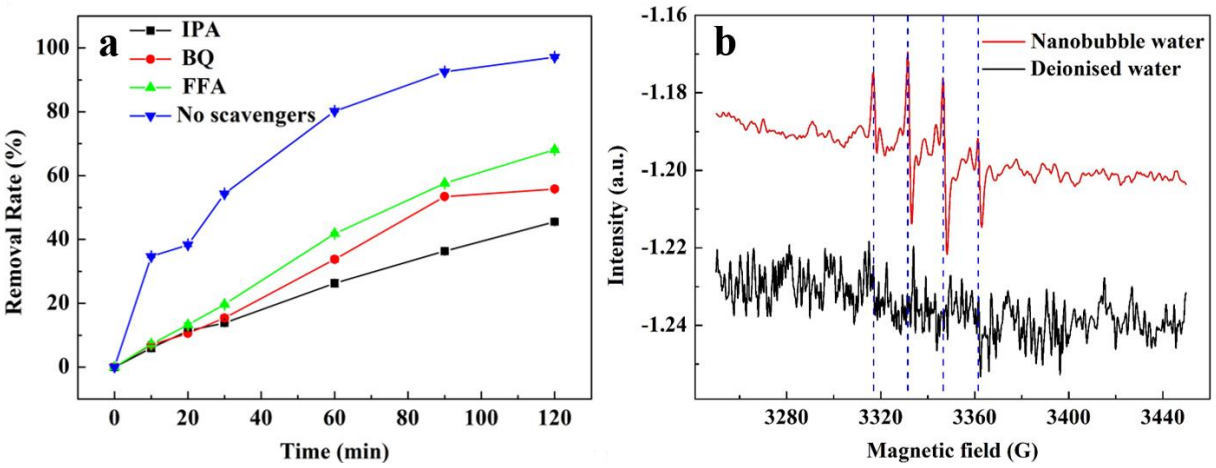


**Fig. 3.** Effect of scavengers on the degradation of RhB (a), ESR evidence of •OH production from oxygen nanobubbles (b).

Further evidences have been presented to demonstrate the formation of •OH radical in the nanobubble system. The generation of •OH with time was monitored and visualized by the three-dimensional EEM spectra with the help of disodium terephthalate (TP) as a fluorescence

probe. A significant peak at the excitation wavelength of 315 nm and an emission wavelength of 425 nm was gradually formed from 0 to 120 min with an increase in the fluorescent intensity (**Fig. 4a-e**). Compared with the nanobubble water without fluorescence probe, there were no peaks at the targeted fluorescent area on EEM spectra (**Fig. S1a-e**). This suggested that the fluorescent adduct, 2-hydroxyterephthalate (TPOH), was formed by the hydroxylation reaction between the added TP and the •OH generated in the nanobubble system (Fang et al., 1996). Furthermore, the •OH radical yield was also quantitatively calculated based on the calibration curves of TPOH (**Fig. S2**) (Soyluoglu et al., 2021; Fang et al., 1996). The results showed that approximately 38.23 nM •OH was generated in the oxygen nanobubble water after stable operation (**Fig. 4f**). However, the productions of $\bullet O_2^-$, and $^1O_2$ were not significantly detected by the probe method (**Fig. 4f**). This finding further confirmed the indispensable role of •OH radical in degrading RhB by oxygen nanobubble treatment.

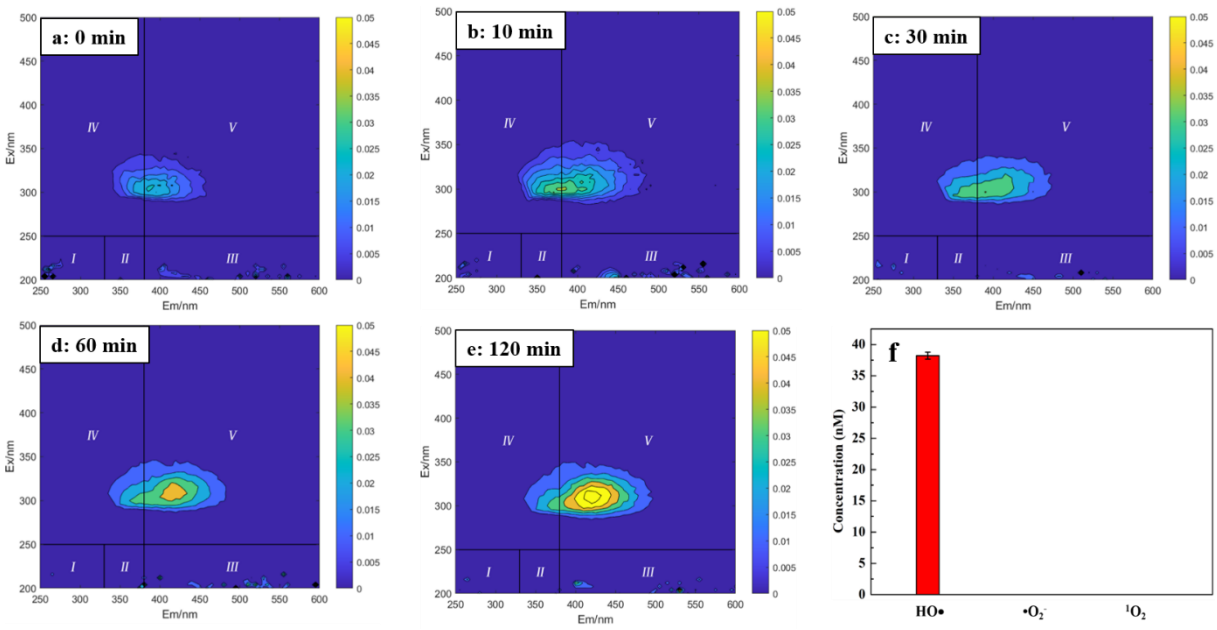


**Fig. 4.** Excitation and emission matrix (EEM) fluorescence spectra of oxygen nanobubble water with the presence of fluorescent probe at different times (a-e) and the concentrations of ROSs generated in the experimental system (f).

It has been calculated that the second order rate constant of RhB with •OH radical is $2.5\times10^{10}$ $M^{-1}s^{-1}$, a value several times higher than other common organic pollutants, like methylene blue ($3.8\times10^{9}$ $M^{-1}s^{-1}$), atrazine ($2.3\times10^{9}$ $M^{-1}s^{-1}$) and carbamazepine ($8.8\times10^{9}$ $M^{-1}s^{-1}$) (Grimme et al., 2010; Xie et al., 2022). This reaction rate is determined by the chemical structure and the

intrinsic properties of the organic compounds. Thus, the combined factors of continuous generation of •OH in the circular reaction system and the high sensitivity of RhB with •OH provide the oxygen nanobubbles with an excellent ability to degrade RhB from the aqueous solution.

### *3.3.2 Degradation pathways of RhB*

For the purpose of a deep understanding of the degradation process, the variation of absorption spectra of degraded RhB in the wavelength of 400-700 nm was detected (**Fig. 5a-c**). The typical absorption band at a wavelength of 554 nm was significantly diminished with the extension of the reaction time, which indicated the chromophore structure (conjugated xanthene ring) of the RhB was gradually destroyed by the oxidative attack of ROSs (Muthusami et al., 2021). In addition, the characteristic peak of RhB at 554 nm exhibited hypsochromic shifts during the reaction (**Fig. 5a-c**). Similar shifts were also observed in previous studies investigating the RhB degradation by photocatalytic processes (He et al., 2009; Zeng et al., 2022). This hypsochromic shift illustrated that the degradation of RhB by oxygen nanobubbles is a chemical N-deethylation process, and a series of N-deethylated intermediates would be generated during the degradation (He et al., 2009).

Furthermore, the potential degradation pathways were speculated based on all the detected intermediates (**Fig. S3** and **Table S3**). Specifically, there were two potential degradation pathways of RhB in this study. The first route was initiated by the N-deethylation process (**Fig. 5d**), where the ethyl group was progressively dissociated from RhB compounds (m/z=443) (Zhang et al., 2018). A series of N-deethylated products were detected in this process, including N, N-diethylrhodamine (DR) (m/z=416), N-ethyl-N-ethylrhodamine (EER) (m/z=388), N-ethyl rhodamine (ER) (m/z=361). Meanwhile, following attack by •OH, the hydroxylation product (m/z= 363) was also formed. Subsequently, the amino, carboxyl, and benzoic acid were wrecked to form intermediates with m/z= 320, 272, and 196. Analogously, the second pathway started with a hydroxylation reaction (**Fig. 5d**). The upper component of the xanthene-containing conjugated structure and lower parts of the benzoic acid of RhB are connected by a single bond, which is easy to break (Wu et al., 2022a). Thus, the benzoic acid component and

the ethyl group of RhB were attacked and replaced by •OH to form a series of hydroxylation intermediates (m/z= 371, 340, 323, and 227). After those intermediates were generated via the two pathways, the conjugated chromophore structure was broken to form products with smaller molecular weights (m/z= 121, 139, 179, and 181). Afterwards, these products were gradually dissociated into simple organic acids or alcohols via a ring-opening reaction (m/z= 60, 114, 136, and 149). Finally, the low molecular weight organics were further mineralized to $CO_2$ and $H_2O$ to realize complete degradation.

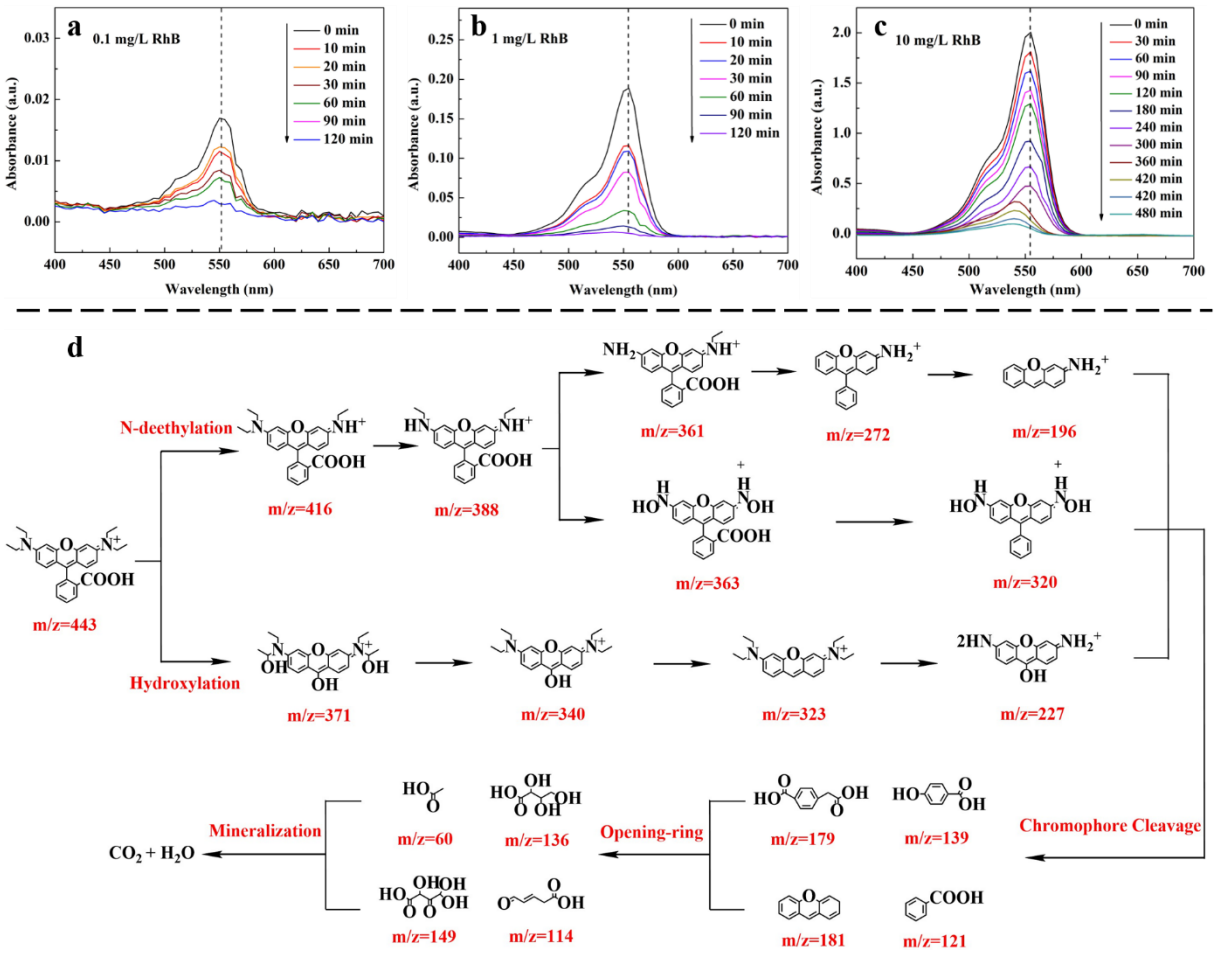


**Fig. 5.** UV-vis absorption spectral variations for RhB with different reaction time under the initial concentrations of 0.1 (a), 1 (b), and 10 (c) mg/L, the potential degradation pathway of RhB by oxygen nanobubbles (d).

## 3.4 Influencing factors on the micropollutant degradation

### *3.4.1 Effect of initial concentrations and the degree of mineralisation*

Following the screen test, the superior oxygen nanobubble treatment approach for the removal of RhB was further studied. For initial concentrations of RhB of 0.1, 1, and 10 mg/L, oxygen

nanobubble treatment could achieve >97% removal in all groups under 90, 120, and 480 min's reaction time, respectively (**Fig. 2c**). The kinetics analysis demonstrated that the RhB degradation process fitted with the pseudo-first-order model ($R^2$>0.90), and the removal rate constant for RhB decreased from 0.036 $min^{-1}$ at 0.1 mg/L to 0.006 $min^{-1}$ at 10 mg/L (**Fig. S4**, **Table S4**). The results showed that the initial concentration affected the degradation rate of RhB by oxygen nanobubble treatment, a result consistent with photocatalysis treatment of RhB (Madima et al., 2022). At a high initial concentration of RhB, the degradation intermediates (by-products) may compete for the consumption of ROSs with the parent RhB compound, leading to a slower reaction rate (Geng and Thagard, 2013). Alternatively, the intermediates with smaller molecular weight may diffuse into the nanobubbles, changing the condition of the bubbles structure (and likely collapse) (Wang et al., 2008), which in turn suppresses the generation of ROSs. Nevertheless, further investigation and/or direct characterisation is needed to confirm these assumptions.

Compared with the removal of RhB by other AOPs, oxygen nanobubble treatment could reach equivalent removal efficiency (>97%) (**Table S4**) (Yu et al., 2021; Zhang et al., 2022). Under the same initial concentration of 1 mg/L, the reaction rate constant of oxygen nanobubble AOP was twice as high as the Fenton-like reactions. However, at an initial concentration of 10 mg/L, the reaction rate constant of the Fenton-like reaction was 2.6 times higher than that of oxygen nanobubbles (**Table S4**). This was mainly caused by the 80 times higher reaction volumes of the oxygen nanobubbles than the Fenton-like reactions listed in the **Table S4**, which led to the 2.6~8.0 times longer reaction time. Furthermore, previous studies on RhB removal normally have typically only assessed the removal efficiency of the parent compound rather than an evaluation of the mineralisation of RhB. In this study, approximately 40%-50% of TOC removal was achieved in all treatment groups with different initial concentrations of RhB under the treatment of oxygen nanobubble (**Fig. 2d**). The results demonstrated that the oxygen nanobubble AOP could not only decolour the RhB-contaminated water, but also provide a significant degree of mineralisation of RhB. However, the optimisation of operation strategies towards the complete degradation of RhB still needs to be studied.

### *3.4.2 Effect of pH and charge neutralization*

The pH of industry effluent varies, which in turn could affect the treatment performance of AOPs (Liu et al., 2021). Therefore, treatment of 1 mg/L RhB by oxygen nanobubbles was carried out at different pH levels (3-10) to assess the effects of the pH on the degradation process. Some differences in RhB removal were identified along with the reactions, however, the final removal rates of RhB in all groups reached 95%±3% and did not exhibit a clear distinction (**Fig. 6a**). The reaction rate constants of all groups fluctuated between 0.023~0.029 $min^{-1}$, without showing a significant difference (**Table S5**). A previous study also found that the pH of solutions did not significantly affect the removal of geosmin and 2-methylisoborneol by oxygen nanobubbles in the pH range of 3-10 (Soyluoglu et al., 2022). Thus, it is evident that oxygen nanobubble technology can play a significant role in degrading RhB from water across a wide range of pH.

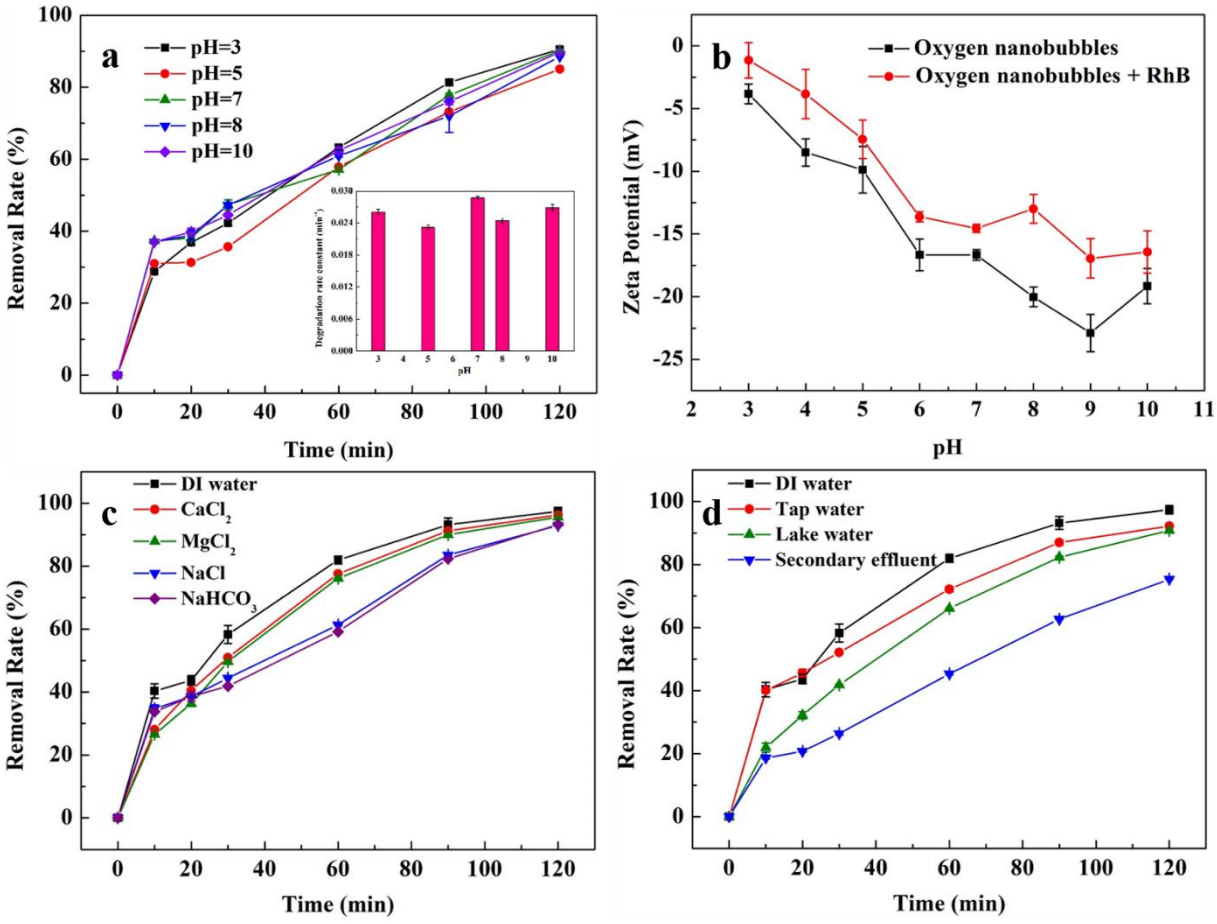


**Fig. 6.** The removal efficiencies of RhB by oxygen nanobubble treatment under initial pH levels of 3-10 (a), the Zeta potential of oxygen nanobubbles before and after reacting with RhB (b), the removal efficiencies of RhB at different background ions (c) and in different real water

samples (d) by oxygen nanobubble treatment.

Part of the stable removal of RhB under different pH conditions may have been due to the characteristics of the negatively charged nanobubbles, which had a negative zeta potential across pH 3-10, decreasing from -3.63 to -22.89 mV from the lowest to highest pH (**Fig. 6b**). The negatively charged surface of the oxygen nanobubbles in this pH range was also observed in other studies (Fan et al., 2021b; Wang et al., 2020). In an acidic solution, excess $H^+$ may attract to the surface of the nanobubbles and increase the zeta potential values, which explains why the bubbles were less negative at low pH. RhB is a typical non-volatile cationic dye, indicating that RhB can mostly exist stably as a cation form in water (Geng and Thagard, 2013). Therefore, the positive-charged RhB would be adsorbed by the negative-charged oxygen nanobubbles and surrounded by the bubble-water interface. The •OH radical and shock waves were indicated to be generated at the gas-liquid interface when bubbles collapse (Agarwal et al., 2011) and contribute directly to the RhB degradation. As a result, after the reactions, the zeta potentials of nanobubbles were increased from 2 to 7 mV in each group and reached -1.16 to -16.95 mV (**Fig. 6b**). This hypothesis was also verified by previous studies showing that the degradation reactions of most non-volatile compounds usually occur not in the interior of the bubbles but on the bubble-solution interface and bulk solution (Hua and Hoffmann, 1996). Thus, it could be inferred that the removal of RhB by oxygen nanobubbles is an interfacial adsorption enhanced ROSs oxidation process.

### *3.4.3 Effect of background ions.*

The presence of various background components in water, such as ionic strength, hardness, and alkalinity, pose significant challenges for ROS-based AOPs in degrading organic micropollutants from water or wastewater (Liao et al., 2001; Yu et al., 2021). Previous studies have also highlighted the impact of foreign ions on the stability of nanobubbles (Soyluoglu et al., 2022). However, the current findings demonstrated that oxygen nanobubble can achieve favourable removal efficiency (exceeding 92%) on RhB when coexisted with 300 mg/L background ions, including $Ca^{2+}$, $Mg^{2+}$, $HCO_3^-$, and $Cl^-$ (**Fig. 6c**). There was no statistical difference ($p > 0.05$) in RhB removal rates, suggesting that existing background ions have negligible impact on the degradation ability of oxygen nanobubble. However, a slight decrease

in the removal rate was observed, and it followed the order of DI water (97.59%) > $CaCl_2$ (96.25%) > $MgCl_2$ (95.58%) > $NaHCO_3$ (93.22%) > NaCl (92.91%) (**Fig. 6c**). The degradation kinetics in all groups was well-fitted with the pseudo-first-order kinetic model, and the degradation constant decreased from 0.028 $min^{-1}$ in DI water to 0.020 $min^{-1}$ in the presence of $NaHCO_3$ and NaCl (**Fig. S5**). The reduction in degradation efficiency of RhB may be attributed to the scavenging effects of the coexisting ions on •OH radical (Devi et al., 2013; Grebel et al., 2010), which inhibit the oxidation capacity of nanobubbles.

Overall, the summary mechanism of RhB degradation by the proposed oxygen nanobubble AOP follows a successive set of distinct phases (**Fig. 7**). In the homogeneous aqueous system, due to the electrical neutralization, the RhB in the cationic form is adsorbed on the liquid-bubble interface by the negatively charged oxygen nanobubbles. Then, the bulk oxygen nanobubbles continuously shrink and eventually collapse to emit significant energy and produce ROSs (•OH, $•O_2^-$, and $^1O_2$). The high redox potential of ROSs, in particular •OH, makes them effectively oxidise RhB. RhB degradation starts from the chemical N-deethylation process, and a series of N-deethylated intermediates are then generated, which can then lead to complete mineralisation of RhB.

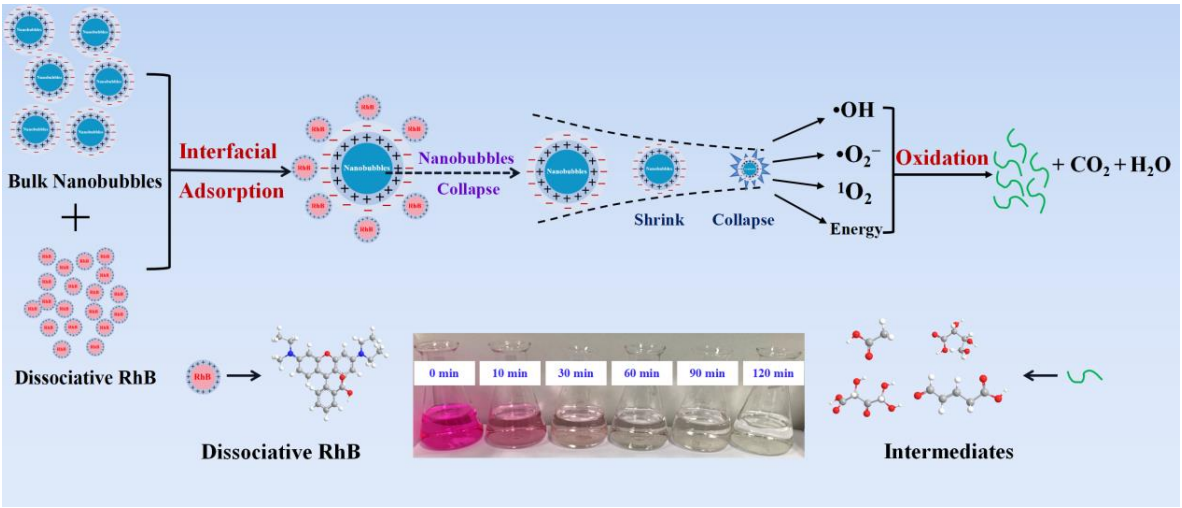


**Fig. 7.** The proposed mechanism of RhB degradation by oxygen nanobubbles.

### 3.5 Validation test in real water samples and engineering implications.

To further test the practical feasibility of nanobubble technology-based AOP, the degradation experiments of RhB were conducted in DI water, tap water, lake water, and secondary effluent

for sewage works. **Table 1** summarised the selected water quality parameters of three real waters. The levels of nitrogen and phosphorus nutrients in secondary effluent were 1.6-2.7 and 1.7-5.0 times higher than the lake water and tap water, respectively. The COD and turbidity also exhibited the trend that secondary effluent > lake water > tap water. The existing inorganic and organic compounds might make the target pollutant more challenging to remove due to the effects of radicals quenching and competitions (Liao et al., 2001; Soyluoglu et al., 2022). The degradation performance of RhB in tap water (92.18%) and lake water (90.78%) exhibited a fair degree of agreement with the removal efficiency in DI water (97.59%) (**Fig. 6d**). Moreover, even though the composition of secondary effluent was more complex, the removal efficiency of RhB could still reach up to 75.32% (**Fig. 6d**). The reduction in the removal rate might be due to the competitions of coexisting organic matters in the authentic waters with RhB compounds on the available ROSs (Soyluoglu et al., 2022). The differences in the COD levels in the three waters support this point (**Table 1**). After oxygen nanobubbles treatment, the COD levels exhibited dramatic decreases of 43%-51% in three water matrices, resulting by the degradation of RhB and other organic matters. Meanwhile, the ammonia and total nitrogen decreased by approximately 15% and 10%, respectively (**Table 1**), due to the potential removal ability of nanobubble technology on ammonia (Wu et al., 2022b). Based on the above results, it was reasonable to identify the oxygen nanobubble-based AOP with a prominent application for RhB removal in authentic effluents.

**Table 1**

Selected water quality parameters of real water samples and RhB removal before and after nanobubble-based AOP treatment.

| | Tap water | | Lake water | | Secondary effluent | |
|---|---|---|---|---|---|---|
| | Before treatment | After treatment | Before treatment | After treatment | Before treatment | After treatment |
| Total phosphorus (mg/L) | 0.14 | 0.13 | 0.29 | 0.30 | 0.48 | 0.46 |
| Labile phosphorus (mg/L) | 0.02 | 0.02 | 0.04 | 0.03 | 0.10 | 0.09 |
| Total nitrogen (mg/L) | 3.5 | 3.1 | 3.7 | 3.4 | 6.1 | 5.3 |
| Ammonia nitrogen (mg/L) | 0.31 | 0.26 | 0.43 | 0.37 | 0.86 | 0.74 |
| COD (mg/L) | 14.1 | 6.8 | 41.3 | 21.1 | 59.5 | 33.9 |

| | | | | | | |
|---|---|---|---|---|---|---|
| Average particle diameter (μm) | <DL | <DL | 23.84 | 23.36 | 66.40 | 63.65 |
| Turbidity (NTU) | 0.12 | 0.09 | 1.59 | 1.36 | 17.92 | 16.22 |
| pH | 7.39 | 7.29 | 7.75 | 7.45 | 7.26 | 7.23 |
| RhB removal (%) | | 92.18% | | 90.78% | | 75.32% |

DL: detection limit

Due to the generation of highly ROSs, AOPs have become an effective approach to degrade organic pollutants with complex macromolecular structures. This study demonstrated a novel and functional-effective AOP technology using oxygen nanobubbles alone without extra solid waste generation and chemicals or precursor addition. Oxygen nanobubbles achieved equivalent removal and mineralization effects on RhB in the homogeneous aqueous system than conventional AOPs through interfacial adsorption enhanced ROSs oxidation process. Notably, compared with RhB, some chemical structures of refractory organic pollutants are more difficult to oxidize, leading to relatively low removal effects when treated by individual nanobubbles. For example, the stable ring structure of geosmin and 2-methylisoborneol makes oxygen nanobubble only achieve <40% removals on them. For those refractory organic pollutants, the integrated approach, combining nanobubble technology with other AOPs may need to be deployed. With the assistance of oxygen nanobubble, the photodegradation efficiency of oxytetracycline was improved from 28% to 60% (Wang et al., 2020). Moreover, the proposed oxygen nanobubble technology not only could promote the efficiency of conventional AOPs in degrading organic pollutants but also has been indicated to be an ideal enhancement method for AOPs with reduction of energy demand and chemical usage. Although the energy and chemical input for nanobubble generation is expected to be much lower than other AOP approaches, the cost-benefit analysis and life cycle assessment of the proposed approach should be carried out in scaled-up studies. In summary, this study provided a green technology of oxygen nanobubble AOP that provides great promise to effectively remove organic micropollutants from water.

## 4. Conclusion

This study has demonstrated that oxygen nanobubble induced AOP can act as an effective and

chemical free additive technology for treating organic micropollutants in both synthetic and real water matrices. The removal efficiency of the model micropollutant Rhodamine B (RhB) treated with oxygen nanobubbles were significantly higher than those treated with air and nitrogen nanobubbles. The initial RhB concentrations (0.1-10 mg/L), pH (3-10), and existing ions ($Ca^{2+}$, $Mg^{2+}$, $HCO_3^-$, and $Cl^-$) exhibited negligible effects on RhB removals by oxygen nanobubble AOP. The electrical neutralization between oxygen nanobubbles and RhB compounds further enhanced the ROSs oxidation on RhB. The •OH was certified as the primary ROS that contributed to RhB degradation through qualitative and quantitative measurement. The potential degradation pathway of RhB involved the processes of N-deethylation, hydroxylation, chromophore cleavage, ring-opening and final mineralization. Moreover, the practical feasibility of nanobubble-based AOP was further validated by the considerable RhB removals (75.3%-90.8%) when treating real water samples, including natural lake water and sewage work's secondary effluent. This work provides a new insight into water and wastewater treatment through an innovative and chemical free oxygen nanobubble AOP.

## Declaration of Competing Interest

The authors declare that they have no known competing financial interests or personal relationships that could have appeared to influence the work reported in this paper.

## Author contributions

**Bangguo Wang:** Investigation, Methodology, Software, Validation, Writing – original draft. **Lijing Wang:** Conceptualization, Investigation, Supervision, Writing – review & editing, Funding acquisition. **Tao Lyu:** Conceptualization, Data verification, Writing – review & editing. **Wenxi Cen:** Formal analysis, Writing – original draft. **Yang Zhang:** Resources, Supervision. **Kaili Zhang:** Resources, Project administration. **Yuanxun Zhang, Yinghui Han and Lei Wang:** Experimental method guidance, Data verification. **Peter Jarvis, Gang Pan and Wei Fan:** Writing – review & editing, Language polishing.

## Acknowledgements

This work was supported by the Industry-Academy cooperation project (E2021000435), National Natural Science Foundation of China (41877310, 22276191, 21976177) and Innovative practice training program for College students of Chinese Academy of Sciences (117900M002). We thank Xuezhen Zhong for assistance in sample characterization.

## References


Agarwal, A., Ng, W.J., Liu, Y., 2011. Principle and applications of microbubble and nanobubble technology for water treatment. Chemosphere 84, 1175-1180. https://doi.org/10.1016/j.chemosphere.2011.05.054.

Ahmed, A.K.A., Shi, X., Hua, L., Manzueta, L., Qing, W., Marhaba, T., Zhang, W., 2018. Influences of air, oxygen, nitrogen, and carbon dioxide nanobubbles on seed germination and plant growth. J. Agric. Food. Chem. 66, 5117-5124. https://doi.org/10.1021/acs.jafc.8b00333.

Akpan, U.G., Hameed, B.H., 2009. Parameters affecting the photocatalytic degradation of dyes using TiO2-based photocatalysts: a review. J. Hazard. Mater. 170, 520-529. https://doi.org/10.1016/j.jhazmat.2009.05.039.

Bui, T.T., Han, M., 2020. Decolorization of dark green Rit dye using positively charged nanobubbles technologies. Sep. Purif. Technol. 233, 116034. https://doi.org/10.1016/j.seppur.2019.116034.

Devi, L.G., Munikrishnappa, C., Nagaraj, B., Rajashekhar, K.E., 2013. Effect of chloride and sulfate ions on the advanced photo Fenton and modified photo Fenton degradation process of Alizarin Red S. J. Mol. Catal. A: Chem. 374-375, 125-131. http://dx.doi.org/10.1016/j.molcata.2013.03.023.

Fan, W., An, W., Huo, M., Xiao, D., Lyu, T., Cui, J., 2021a. An integrated approach using ozone nanobubble and cyclodextrin inclusion complexation to enhance the removal of micropollutants. Water Res. 196, 117039. https://doi.org/10.1016/j.watres.2021.117039.

Fan, W., Cui, J., Li, Q., Huo, Y., Xiao, D., Yang, X., Yu, H., Wang, C., Jarvis, P., Lyu, T., Huo, M., 2021b. Bactericidal efficiency and photochemical mechanisms of micro/nano bubble-enhanced visible light photocatalytic water disinfection. Water Res. 203, 117531. https://doi.org/10.1016/j.watres.2021.117531.

Fang, X.W., Mark, G., Sonntag, C., 1996. OH radical formation by ultrasound in aqueous solutions Part I the chemistry underlying the terephthalate dosimeter. Ultrason. Sonochem. 3, 57-63. https://doi.org/10.1016/1350-4177(95)00032-1.

Geng, M., Thagard, S.M., 2013. The effects of externally applied pressure on the ultrasonic degradation of Rhodamine B. Ultrason. Sonochem. 20, 618-625. https://doi.org/10.1016/j.ultsonch.2012.08.002.

Grebel, J.E., Pignatello, J.J., Mitch, W.A., 2010. Effect of halide ions and carbonates on organic contaminant degradation by hydroxyl radical-based advanced oxidation processes in saline waters. Environ. Sci. Technol. 44, 6822-6828. https://doi.org/10.1021/es1010225.

Grimme, S., Antony, J., Ehrlich, S., Krieg, H., 2010. A consistent and accurate ab initio parametrization of density functional dispersion correction (DFT-D) for the 94 elements H-Pu. J. Chem. Phys. 132, 154104. https://doi.org/10.1063/1.3382344.

He, Z., Sun, C., Yang, S., Ding, Y., He, H., Wang, Z., 2009. Photocatalytic degradation of rhodamine B by Bi(2)WO(6) with electron accepting agent under microwave irradiation: mechanism and pathway. J. Hazard. Mater. 162, 1477-1486. https://doi.org/10.1016/j.jhazmat.2008.06.047.

Hernandez, C., Abenojar, E.C., Hadley, J., de Leon, A.C., Coyne, R., Perera, R., Gopalakrishnan, R., Basilion, J.P., Kolios, M.C., Exner, A.A., 2019. Sink or float? Characterization of shell-stabilized bulk nanobubbles using a resonant mass measurement technique. Nanoscale 11, 851-855. https://doi.org/10.1039/C8NR08763F.

Hu, L., Xia, Z., 2018. Application of ozone micro-nano-bubbles to groundwater remediation. J. Hazard. Mater. 342, 446-453. https://doi.org/10.1016/j.jhazmat.2017.08.030.

Hua, I., Hoffmann, M.R., 1996. Kinetics and mechanism of the sonolytic degradation of $CCl_4$: intermediates and byproducts. Environ. Sci. Technol. 30, 864-871. https/3TBFNeWp0PiPoJUsZ6QlmyaOyR/10.1021/es9502942.

Ji, X., Liu, C., Pan, G., 2020. Interfacial oxygen nanobubbles reduce methylmercury production ability of sediments in eutrophic waters. Ecotoxicol. Environ. Saf. 188, 109888. https://doi.org/10.1016/j.ecoenv.2019.109888.

Lee, H., Park, S.H., Park, Y.K., Kim, B.H., Kim, S.J., Jung, S.C., 2013. Rapid destruction of the rhodamine B using $TiO_2$ photocatalyst in the liquid phase plasma. Chem. Cent. J. 7, 156. http://journal.chemistrycentral.com/content/7/1/156.

Li, P., Takahashi, M., Chiba, K., 2009. Degradation of phenol by the collapse of microbubbles. Chemosphere 75, 1371-1375. https://doi.org/10.1016/j.chemosphere.2009.03.031.

Liao, C.H., Kang, S.F., Wu, F.A., 2001. Hydroxyl radical scavenging role of chloride and bicarbonate ions in the $H_2O_2$/UV process. Chemosphere 44, 1193-1200. https://doi.org/10.1016/S0045-6535(00)00278-2.

Liu, P., Zhong, D., Xu, Y., Zhong, N., He, G., 2021. Co/Fe co-doped porous graphite carbon derived from metal organic framework for microelectrolysis-Fenton catalytic degradation of Rhodamine B. J. Environ. Chem. Eng. 9, 105924. https://doi.org/10.1016/j.jece.2021.105924.

Liu, S., Oshita, S., Kawabata, S., Makino, Y., Yoshimoto, T., 2016. Identification of ROS produced by nanobubbles and their positive and negative effects on vegetable seed germination. Langmuir 32, 11295-11302. https://doi.org/10.1021/acs.langmuir.6b01621.

Lyu, T., Wu, S., Mortimer, R.J.G., Pan, G., 2019. Nanobubble technology in environmental engineering: revolutionization potential and challenges. Environ. Sci. Technol. 53, 7175-7176. https://doi.org/10.1021/acs.est.9b02821.

Madima, N., Kefeni, K.K., Mishra, S.B., Mishra, A.K., Kuvarega, A.T., 2022. Fabrication of magnetic recoverable $Fe_3O_4$/$TiO_2$ heterostructure for photocatalytic degradation of rhodamine B dye. Inorg. Chem. Commun. 145, 109966.

https://doi.org/10.1016/j.inoche.2022.109966.
Murtaza, S.Z.M., Alqassem, H.T., Sabouni, R., Ghommem, M., 2023. Degradation of micropollutants by metal organic framework composite-based catalysts: A review. Environ. Technol. Innovation. 2023; 29, 102998. https://doi.org/10.1016/j.eti.2022.102998.
Muthusami, R., Ramachandran, V., Palaniappan, M., Arumugam, S., Palanisamy, K., Irena, K., Rangappan, R., 2021. Cu(II) Schiff base complex functionalized mesoporous silica nanoparticles as an efficient catalyst for the synthesis of questiomycin A and photo-Fenton-like rhodamine B degradation. J. Solid State Chem. 302, 122429. https://doi.org/10.1016/j.jssc.2021.122429.
Soyluoglu, M., Kim, D., Zaker, Y., Karanfil, T., 2021. Stability of oxygen nanobubbles under freshwater conditions. Water Res. 206, 117749. https://doi.org/10.1016/j.watres.2021.117749
Soyluoglu, M., Kim, D., Zaker, Y., Karanfil, T., 2022. Removal mechanisms of geosmin and MIB by oxygen nanobubbles during water treatment. Chem. Eng. J. 443, 136535. https://doi.org/10.1016/j.cej.2022.136535.
Thi Phan, K.K., Truong, T., Wang, Y., Bhandari, B., 2020. Nanobubbles: Fundamental characteristics and applications in food processing. Trends Food Sci. Technol. 95, 118-130. https://doi.org/10.1016/j.tifs.2019.11.019.
Tran, C.V., La, D.D., Thi Hoai, P.N., Ninh, H.D., Thi Hong, P.N., Vu, T.H.T., Nadda, A.K., Nguyen, X.C., Nguyen, D.D., Ngo, H.H., 2021. New $TiO_2$-doped Cu-Mg spinel-ferrite-based photocatalyst for degrading highly toxic rhodamine B dye in wastewater. J. Hazard. Mater. 420, 126636. https://doi.org/10.1016/j.jhazmat.2021.126636.
van Gijn, K., Zhao, Y., Balasubramaniam, A., de Wilt, H.A., Carlucci, L., Langenhoff, A.A.M., Rijnaarts, H.H.M., 2022. The effect of organic matter fractions on micropollutant ozonation in wastewater effluents. Water Res. 222, 118933. https://doi.org/10.1016/j.watres.2022.118933.
Wang, L., Ali, J., Wang, Z., Oladoja, N.A., Cheng, R., Zhang, C., Mailhot, G., Pan, G., 2020. Oxygen nanobubbles enhanced photodegradation of oxytetracycline under visible light: Synergistic effect and mechanism. Chem. Eng. J. 388, 124227. https://doi.org/10.1016/j.cej.2020.124227.
Wang, L., Miao, X., Ali, J., Lyu, T., Pan, G., 2018. Quantification of oxygen nanobubbles in particulate matters and potential applications in remediation of anaerobic environment. ACS Omega. 3, 10624-10630. https://doi.org/10.1021/acsomega.8b00784
Wang, X., Wang, J., Guo, P., Guo, W., Li, G., 2008. Chemical effect of swirling jet-induced cavitation: degradation of rhodamine B in aqueous solution. Ultrason. Sonochem. 15, 357-363. https://doi.org/10.1016/j.ultsonch.2007.09.008.
Wu, Y., Kong, L.H., Shen, R.F., Guo, X.J., Ge, W.T., Zhang, W.J., Dong, Z.Y., Yan, X., Chen,

Y., Lang, W.Z., 2022a. Highly dispersed and stable Fe species supported on active carbon for enhanced degradation of rhodamine B through peroxymonosulfate activation: Mechanism analysis, response surface modeling and kinetic study. J. Environ. Chem. Eng. 10, 107463. https://doi.org/10.1016/j.jece.2022.107463.

Wu, Y., Lyu, T., Yue, B., Tonoli, E., Verderio, E.A.M., Ma, Y., Pan, G., 2019. Enhancement of tomato plant growth and productivity in organic farming by agri-nanotechnology using nanobubble oxygation. J. Agric. Food Chem. 67, 39, 10823-10831. https://libyw.ucas.ac.cn/https/3TBFNeWp0PiPuP8cpgVHmNyjTl/10.1021/acs.jafc.9b04117.

Wu, Y., Tian, W., Zhang, Y., Fan, W., Liu, F., Zhao, J., Wang, M., Liu, Y., Lyu, T., 2022b. Nanobubble technology enhanced ozonation process for ammonia removal. Water 14, 1865. https://doi.org/10.3390/w14121865.

Xia, C., Ye, H., Wu, Y., Garalleh, H.A., Garaleh, M., Sharma, A., Pugazhendhi, A., 2023. Nanofibrous/biopolymeric membrane a sustainable approach to remove organic micropollutants: A review. Chemosphere 314, 137663. https://doi.org/10.1016/j.chemosphere.2022.137663.

Xie, Z.H., He, C.S., Zhou, H.Y., Li, L.L., Liu, Y., Du, Y., Liu, W., Mu, Y., Lai, B., 2022. Effects of molecular structure on organic contaminants' degradation efficiency and dominant ROS in the advanced oxidation process with multiple ROS. Environ. Sci. Technol. 56, 8784−8795. https://doi.org/10.1021/acs.est.2c00464.

Yang, Y., Zhang, X., Jiang, J., Han, J., Li, W., Li, X., Leung, K.M.Y., Snyder, S.A., Alvarez, P.J.J., 2022. Which micropollutants in water environments deserve more attention globally? Environ. Sci. Technol. 56, 13-29. https://doi.org/10.1021/acs.est.1c04250.

Yu, H., Liu, Y., Xu, M., Cong, S., Liu, M., Zou, D., 2021. Hydroxylamine facilitated heterogeneous fenton-like reaction by nano micro-electrolysis material for rhodamine B degradation. J. Cleaner Prod. 316, 128136. https://doi.org/10.1016/j.jclepro.2021.128136.

Zeng, Y., Xu, Y., Zhong, D., Yao, H., Zhong, N., 2022. Peroxymonosulfate activated by photocatalytic fuel cell with g-$C_3N_4$/BiOI/Ti photoanode to enhance rhodamine B degradation and electricity generation. J. Hazard. Mater. 425, 127967. https://doi.org/10.1016/j.jhazmat.2021.127967.

Zhang, H., Lyu, T., Liu, L., Hu, Z., Chen, J., Su, B., Yu, J., Pan, G., 2021. Exploring a multifunctional geoengineering material for eutrophication remediation: Simultaneously control internal nutrient load and tackle hypoxia. Chem. Eng. J. 406, 127206. https://doi.org/10.1016/j.cej.2020.127206.

Zhang, J., Yan, M., Sun, G., Li, X., Hao, B., Liu, K., 2022. Mg-Fe-Al-O spinel: Preparation and application as a heterogeneous photo-Fenton catalyst for degrading Rhodamine B. Chemosphere 304, 135318. https://doi.org/10.1016/j.chemosphere.2022.135318.

610 Zhang, Y., Zhou, J., Cai, W., Zhou, J., Li, Z., 2018. Enhanced photocatalytic performance and
611 degradation pathway of Rhodamine B over hierarchical double-shelled zinc nickel oxide
612 hollow sphere heterojunction. Appl. Surf. Sci. 430, 549-560.
613 https://doi.org/10.1016/j.apsusc.2017.06.325.